Tissue and Cell 76 (2022) 101758

Contents lists available at ScienceDirect

Tissue and Cell

journal homepage: www.elsevier.com/locate/tice

Inhibition of gene expression and production of iNOS and TNF-α in experimental model of neurodegenerative disorders stimulated microglia by Soy nano-isoflavone/stem cell-exosomes

Eman Mohamed Faruk [a,b,*], Hanan Fouad [c,d], Rehab Abd Allah Hasan [e], Neama Mahmoud Taha [f], Amal Mahmoud El-Shazly [g]

[a] Department of Anatomy, Faculty of Medicine, Umm Al-Qura University, Makkah, Saudi Arabia
[b] Department of Histology & Cell Biology, Faculty of Medicine, Benha University, Egypt
[c] Medical Biochemistry & Molecular Biology, Faculty of Medicine, Cairo University, Egypt
[d] Galala University, Faculty of medicine, Suez Governorate, Egypt
[e] Department of Histology & Cell Biology, Faculty of Medicine for Girls; AFMG, Al-Azhar University Egypt
[f] Department of physiology, Umm Al-Qura University, Makkah, Saudi Arabia
[g] Department of Anatomy, Faculty of Medicine, Benha University, Egypt

ARTICLE INFO

Keywords:
Neurodegenerative disease
Soy isoflavones
Mesenchymal stem cells exosomes
TNF-α
iNOS
Gene expression

ABSTRACT

The present study evaluated the therapeutic potential of soybean nano-isoflavone extract versus bone marrow mesenchymal stem cells derived extracellular exosomes (BMSCs-EXs) in experimentally induced neurodegenerative diseases in rats (ND). In this study, 36 albino male rats were divided into four groups: Group I (control rats); Group II (induced neurodegenerative disease in rats by intraperitoneal injection of D-galactose (120 mg/kg/day for 2 months); Group III (ND-induced rats treated with nano-isoflavone in doses of 10 mg/kg by oral gavage for 3 months); and Group IV (ND-induced rats treated with a single dose injection of BMSCs-EXs. The effect of BMSCs-EXs was evaluated by cerebral oxidant/antioxidant biomarkers, and mRNA gene expression quantitation for cerebral tumor necrosis factor α (TNF-α), inducible nitric oxide synthase (i-NOS) and GAPDH pathway-encoding genes by real time reverse transcription polymerase chain reaction (RT-PCR) techniques. Then, histopathological examination of the cerebral cortical tissues. Our results showed that BMSC-EXs were successfully isolated and characterized. D-galactose produced a significant rise in the number of damaged neurons, decreased cerebral superoxide dismutase and catalase activities, increased cerebral malondialdehyde levels, downregulated the cerebral TNF-α, and i-NOS pathway-encoding genes. Furthermore, BMSC-EXs and nano-isoflavone treatments repaired damaged cerebral tissue and recovered its function greatly following induction of neurodegenerative disease. Treatment with either MSCs-EXs or nano-isoflavones led to significant improvement in the histological findings, reversed the degenerative effect of D-galactose, and had a favorable therapeutic utility against D- galactose-induced neurodegenerative disease.

1. Introduction

The term neurodegenerative disease (ND) describes a variety of diseases characterized by progressive deterioration in the histology or physiology of the central nervous system or peripheral nervous system. The two most prevalent neurodegenerative diseases (NDs) are Alzheimer's disease and Parkinson's disease (Lepeta et al., 2016a).

By increasing the lifespan of populations, the incidence of NDs is increasing. According to the United Nations statement on world population aging (2017), the projected universal population aged 60 years or older in 2017 was 962 million, and this number is projected to double by 2050. Improvement of effective neuroprotective therapies is therefore a key research area; on the other hand, this requires a thorough understanding of the etiopathogenesis of the diseases. (United Nations DoEaSA, 2017)

Different parts of the brain are affected by neurodegenerative diseases, resulting in sensory, motor, and cognitive impairments (Woolley et al., 2011; Montero-Odasso et al., 2017). Identifying the various

* Corresponding author at: Medical Histology & Cell Biology, Faculty of Medicine, Banha University, a POB 11562, Egypt.
E-mail addresses: emkandel@uqu.edu.sa, faruk_eman@yahoo.com (E.M. Faruk).

https://doi.org/10.1016/j.tice.2022.101758
Received 20 October 2021; Received in revised form 2 February 2022; Accepted 9 February 2022
Available online 11 February 2022
0040-8166/

neurodegenerative disorders clearly may lead to therapeutic advances if we recognize their similarities (Vadakkan, 2016; Hervas et al., 2012). Symptoms of neurodegeneration include neuronal loss, deposition of intracellular protein molecules, and intercellular disruption of the whole system (Gitler et al., 2017).

In animal models, D-galactose (DG) is commonly used to induce brain aging. DG-induced brain aging is associated with mitochondrial dysfunction, inflammation, apoptosis, increased oxidative stress, and decreased brain neurotrophic factors. This results in impaired cognitive functions (Ali et al., 2015). Accumulation of DG in neuronal cells initiates the reaction with the amino groups of proteins and the formation of glycation end products (GE), which is the leading cause of pathological complications of several diseases as in diabetes, atherosclerosis, nephropathy and neurodegenerative disorders (Shwe et al., 2018).

Isoflavones are organic biomolecules linked to flavonoids and have estrogenic properties (Rong et al., 2019). Soybeans and soy products contain isoflavones such as glycitein, daidzein, and genistein, as well as their glycosides (Bhatt et al., 2018). The soy isoflavones were found to protect against the cognitive impairment induced by amyloid-beta (Aβ) peptide in rats. Isoflavones prevent oxidative stress induced by Aβ-peptide in neuronal cells by activation of Nrf2 signaling pathway (Devi et al., 2017). Genistein constitutes up to 50 % of the total isoflavones and was reported to exert efficient neuroprotective functions (Go et al., 2016).

Bone marrow stem cells derived extracellular exosomes (BMSCs-EXs) have potential therapeutic effects like BMSCs. BMSCs-EXs have emerged as a promising therapeutic approach for the treatment of neurodegenerative disease (Cui et al., 2019).

The current study examined the effects of soybean nano-isoflavone supplementation or BMSC-EXs on experimental neurodegenerative disorders models in rats.

2. Materials and methods

2.1. Animals, groups, study design, and dosing

Thirty-six male-albino rats (about 200–250-g), whose age ranged from seven to nine weeks were bred in the animal experimental unit of Faculty of Medicine for Girls, Al-Azhar University, Cairo, Egypt. Upon approval from the Local Ethical Board for the investigational use of research laboratory animals (Approval Number IORG0010305). The rats were kept inside clean stainless-steel cages with the ideal circumstances of the Established Guideline for Concern and Use of Laboratory Animals. The animals were acclimatized to the laboratory conditions for one week before the experiment and housed in properly ventilated cages under standard conditions of twelve hours dark/light cycles, providing them with water and food adlibitum. All ethical protocols were supervised and followed by the animal facilities for animal treatment. The experimental protocol was approved by the Ethical Committee (Institutional Animal Care Committee). Treatments were prepared and coded based on the randomization schemes by experimenters who knew the codes but were otherwise not involved in any of the experiments or data analysis. Coded results after each experiment were sent to the biostatistician for analysis. Therefore, Biostatistician, Technicians and Behavioral assessor investigator were blinded to the experimental conditions of the animals. Unblinding was performed only after all statistical analyses were completed. The complete set of data is reported, and no exclusions of any data points were made. The image analysis and the data obtained were exposed to statistical analysis which were carried out by an expert who is unaware of the experimental groups to eliminate experimental biases that arise from the investigator's expectations and, observer bias.

Animals were categorized into the following-groups (n = 9/-group):

Group I served as a negative control group and were not subjected to any procedure.

Group II served as the pathological control group (neurodegenerative disorders group) that was intraperitoneally injected with D-galactose (120 mg/ kg/ daily dissolved in 0.9 % saline for 2 months) [9&10].

Group III served as the isoflavone-treated group that was given oral gavage of soy nano isoflavone extract (10 mg/kg for 3 months) after induction of the neurodegenerative disorders model as in group II. The contents and constituents of Isoflavone-rich soy isolates were previously described (Lepeta et al., 2016a; Go et al., 2016).

Group IV served as BMSCs-EXs treated group that was intravenously injected through caudal vein with a single dose of BMSCs-EXs (the dose was adjusted to 100 μg protein/suspended in 0.5 mL PBS) after induction of the neurodegenerative disease model (Cui et al., 2019). BMSC-EXs pellet protein content was quantified by Bradford method (BioRad, Hercules, CA, USA).

2.2. Soybean isoflavones and used chemicals

D-Galactose was purchased from Sigma Alrich (Cat No. G0750-1KG) dissolved in 0.9 % saline at concentrations of 20 mg/mL. Soybean isoflavones were purchased from Sigma-Aldrich Chemicals, Germany (Cat No. of isoflavone mixture: S9633-500 G, G6776-10MG, 30408-5MG, and G2785-7MG). Soy-nano-isoflavone was prepared and supplied by Dr. Mohammed A.S. Abourehab, Faculty of Pharmacy, Minia University, Egypt, as previously described (Zhang et al., 2019).

2.3. Soy nano-isoflavone characterization study (Size of particle (SP), particle distribution index (PDI), and Saturation solubility)

Mean size of particle of the soy nano-isoflavone formulation (SP) and particle distribution index (PDI) i.e studying the uniform distribution of all particles in the formulation) were measured by using Malvern Zetasizer Nano ZS (Malvern Instruments, UK) and for three-dimensional analysis of the particles from multiple angles scanning electron microscope (SEM) (JEOL JSM-6700F, Egypt) and transmission electron microscope were used as described by (Boiko et al., 2020), while saturation solubility was measured by subjected of soy nano-isoflavone to centrifugation (3000 rpm for 30 min). All were done in National Research Center, Dokki, Egypt.

2.4. BMSCs isolation and ex vivo expansion

Preparation, isolation, and identification of rat BM-MSCs and BMSC-EXs were conducted in the Stem Cell Unit of Biochemistry and Molecular Biology at Medical Biochemistry Department, Faculty of Medicine, Kasr Al-Ainy University, Egypt.

Male albino rats (7 weeks old and 150–200 g) were euthanized and slaughtered by cervical displacement. Bone marrow cells were picked by washing the tibia and femur in sterile phosphate buffer saline (PBS), then resuspension of cells after centrifugation by alpha-Minimum Essential Medium (alpha MEM) complemented by 10 % fetal bovine serum and 80 μg/mL gentamicin then plated at a density of 106 viable nucleated cells/cm2. Non adherent cells were thrown away after three days by changes its media. When cells achieved convergence, adherent viable cells were disconnected by using 2.65 mM EDTA with 0.25 % trypsin then subjected to centrifugation, the next subculture at 7.000 cells/cm2 was done. After two passages, adherent MSCs were identified and transplanted (Baghaei et al., 2017). All chemicals and reagents used in BMSCs isolation and expansion were supplied from ThermoFisher Scientific (USA). To exclude contamination of the serum-derived exosomes, serum was used for propagation of cell cultures and the collection of supernatants was clarified by ultracentrifugation at 100,000× *g* for 18 h (Chernyshev et al., 2021).

2.5. Immunophenotyping of BMSCs

Immunophenotyping was conducted by flow cytometry with immuno- staining by monoclonal antibodies against CD29

(unconjugated, R&D Systems Cat No. MAP17781)-and a CD44 a (PE-conjugated, R&D Systems Cat No. FAB3660P) as positive markers and monoclonal antibodies against CD34 (APC-conjugated, R&D systems, Cat No. FAB7227A) and CD45 (R&D Systems, Cat No. MAB1430) as negative markers (Gorgun et al., 2019).

2.6. Adipogenic and osteogenic differentiation potential of BMSCs

BMSCs differentiation, osteogenic, and adipogenic possibility was evaluated once cell display to the typical osteogenic and adipogenic diversity protocols for two to three weeks as previously described (Scuteri et al., 2014)·

2.7. Isolation of BMSC-derived Exosomes (BMSCs-EXs)

In brief, BMSCs-EXs were separated from the supernatants of second and third passages of BMSCs supplement with α-MEM containing exosome-depleted FBS (FBS, GE Healthcare, Amersham, U.K.) where 6×10^6 BMSCs were seeded in 25 mL exosome-depleted medium and incubated for 72 h. Centrifugation at 2000×*g* for 20 min was done to remove the debris. The exosomes were removed by Centrifugation at 100,000×*g* for 1 h at 4 °C for the cell-free supernatant by using ultra-centrifuge of Beckman Coulter Optima L-90 K (AQ11). For the removal of microvesicles and apoptotic bodies larger than 200 nm, the supernatant was passed through a filter with a pore size of 0.22 μm. The pellet was washed by serum-free medium and by N-2-Hydroxy Ethyl Piperazine-N′-2-Ethane Sulfonic acid (HEPES) 25 mM (Sigma Aldrich, USA), then an ultracentrifugation was employed for the second pellet under the same conditions (Théry et al., 2006). The protein contents of the exosomes were controlled using the Bradford protocol (Bio-Rad, Hercules, Cat No 5000205, California, USA). A total 20 T75 flasks of BMSCs (~ 20×10^6 cells) were used to achieve the final ~100 μg exosomes that were resuspended in 0.5 ml PBS (Yentrapalli et al., 2017; Nassar et al., 2016).

2.8. Detection and identification of BMSCs-EXs

Flowcytometry was done by using Activated Fluorescence Cell Sorting (FACS). The FITC conjugated bodies, CD73, CD44 (Becton Dickinson, FACSa Calibur), CD63 (Miltenyi Biotec, Bergisch Gladbach, German) were utilized2.Also, to identify the homing of BMSCs EXs into the rat brain tissue (Faruk et al., 2018; Shahror et al., 2019). PKH26 Red (Fluorescent Cell Linker Kit) was used to label BMSCs-EXs (Sigma Aldrich, USA, MIN126), and then the labelled BMSCs-EXs were injected into the tail vein of rats with ND. Brain tissues were examined by fluorescence microscope to visualize homing of PKH26 stained BMSCs-EXs that localize in brain tissues. In addition, BMSCs-EXs were characterized by transmission electron microscope (TEM) in which BMSCs-EXs were fixed with 2.5 % glutaraldehyde for 2 h, after being washed, EXs were ultra-centrifuged and suspended in 100 μL human serum albumin (HSA). A total of 20 μL of EXs were loaded onto a formvar/carbon-coated grid, negatively stained with 3% aqueous phosphor-tungstic acid for 1 min and observed by TEM (HITACHI, H-7650, Japan), which showed their spheroid morphology andconfirmed their nano-size.

2.8.1. Behavioral studies Morris water maze test

For assessing the learning ability and its memory, this test is based on the presence of a circle water pool and 4 spaced equal points around the edge of the water pool were designed and dark platforms covered the water pool. Rat was given a maximum time about two and a half minutes to identify the platform that allows the animal to escape the water by using various cues. The results for escape latency have been presented as mean ± SEM (Sawyer et al., 2017).

2.9. Biochemical assay of oxidative enzymes

The left hemispheres were washed with PBS and 1 gm of brain tissues were homogenized with 5 ml ice-cold saline by using a sonic homogenizer and 10 % of homogenate tissue was put in 50 mm PBS solution (pH 7.4). Brain tissues were subjected to centrifugation at 4000 rpm for15-min and the supernatants were collected and used for biochemical assays. Commercial kits used according to the manufacturer's recommendations for determination of glutathione (GSH, Thermofisher Scientific, Cat No. EIAGSHC), superoxide dismutase (SOD, Thermofisher scientific, Cat No.- EIASODC), malondialdehyde (MDA, Abcam-Cat No. ab118970), and catalase (CAT, Thermofisher Scientific, Cat No. EIACATC).

2.10. Assay of gene expression levels of TNF-α, iNOS, and GAPDH

Gene expression level of TNF-α, iNOS (NOS2), and GAPDH was conducted by real- time PCR using StepOnePlus Real-Time PCR system (Applied Biosystems, USA). Tissues were analyzed for total RNAs by utilizing RNA assay Mini Kit (Qiagen, USA, Cat No./ID: ID: 74104). Then spectrophotometry (JENWAY, USA) was used for quantified of extracted RNAs at 260 nm.

2.11. Primer sequence

PCR-primers were designed by using Primer-Blast software from the subsequent website: http://www.ncbi.nlm.nih.gov/tools/primer-blast Ideal primer pairs were selected considering the melting temperature to be (Tm: 60–65-°C) and PCR product length about (90–200 bp) shown in Table 1.

2.11.1. Real-time quantitative PCR using SYBR green

Software version 3.1 (Applied Biosystems, USA) was used for analysis of Step One plus real-time PCR system. The annealing temperature was controlled for the primer sets and the PCR protocol. All clonal (cDNA) was organized for glyceraldehyde 3-phosphatea dehydrogenase (GAPDH), the entire gene markers, and non-template negative control. Five microliters of full RNA were utilized to create cDNA using 20 pmol antisense primer and 0.8-μL AMV reverse transcriptase for 60 min at 37 ℃. The mRNA genus was measured by utilizing the SYBR® Green-method (Applied- Biosystems, CA, USA). Hardening temperature of 60 ℃ was controlled for the entire primer sets. Real time polymerase reactions were done in 25 μL of Mater Mix of SYBR Green, 3 μL of cDNA, 900 nmol/L of each primer. Magnification situation was done corresponding to the company requirements: 2 min at 50 ℃ then 10 min at 90℃, and 10 min at 60℃ (40 repeated cycles with 15 s denaturation).

2.12. Relative quantification calculation (relative expression)

The expressions of all studied genes were measured by utilizing the comparative Cycle threshold (Ct) way. The data collected for PCR result Ct values of the object genes and the house keeping gene; GAPDH. No template cDNA was included in the negative control sample. Data were

Table 1
Oligonucleotide primers sequences used in the quantitative polymerase chain reaction (PCR) measurements for the GAPDH, TNF α, and NOS3.

NM_000594.4 Tumor necrosis factor (TNF α), mRNA
Sense-primer- 5′- AGAACTCACTGGGGCCTACA-3′
Antisense-primer 5′- GCTCCGTGTCTCAAGGAAGT-3′
NG_011992.1 Nitric synthase (NOS3), mRNA
Sense-primer. - 5′- TCTTGCTAACTCTGGCGCAC-3
Antisense-primer- 5′- AAGAAGTGGCATCAAGCGGA-3′
XR: 598347.1 Glyceraldehyde 3- phosphate dehydrogenase (GAPDH)
Sense-primer. - 5′- GATGCTGGTGCTGAGTATGTCG -3′
Antisense-primer 5′- GTGGTGCAGGATGCATTGCTGA -3′

Table 2
Soy nano-isoflavone characterization diameter(nm), intensity % and width(nm).

Parameters/groups	Diameter(nm)	Intensity %	Width (nm)
Peak 1	249.1	96,9	107.4
Peak 2	5321	1.2	746.8
Peak 3	0.000	0.0	0.000

measured using the Applied-Biosystems StepOneplus™ software. GAPDH housekeeping gene was used for standardization of the results of the target genes that were resulted as fold changes relative to the control sample background level.

2.12.1. Histological and immunohistochemically study

After termination of the experiment, animals were injected with thiopental sodium intraperitoneally (100 mg/kg). The right hemispheres (frontal lobes) of each brain were taken. Fixation was done by 10 % buffered formalin (Bancroft and Layton, 2013). Paraffin serials of 5 mm thickness sections were done and stained with H&E (Kumar and Kiernan, 2010) and silver impregnation (for neurofibers) (Jackson and Blythe, 2013). Sections were processed with the avidin biotin peroxidase complex for immunohistochemical analysis to identify the intermediate filament protein (glial fibrillary acidic- protein (GFAP) that is positively expressed in the astrocytes of the cerebral cortex and used for detection of astrocytes. Monoclonal antiglial fibrillary acidic protein (GFAP) antibodies at 1: 400 dilutions were used (Sigma-Aldrich, St. Louis, Missouri, USA). Antigen retrievals were done by steam heating the slides in 1 mmol/L EDTA solution for 30 min. Endogenous biotin was blocked, then staining was conducted by the automated immunostainer (DAKO) (Xu et al., 2007). CD68 immunostaining was examined to showed cells of the macrophage/monocyte lineage, which are also present in microglia. CD68 antibody (clone KP1, Dako Corporation, Carpinteria, California, USA) was utilized at a dilution of 1:50 then counterstained with Mayer's hematoxylin. Cytoplasm's of Microglia were stained positive with CD68. The positive cells that were used as control positive cells were the Liver Kupffer cells while the negative control cells were showed by neglecting the primary antibody step; accordingly, no immunostaining showed, and CD68 positive cells were appeared brown in colors.

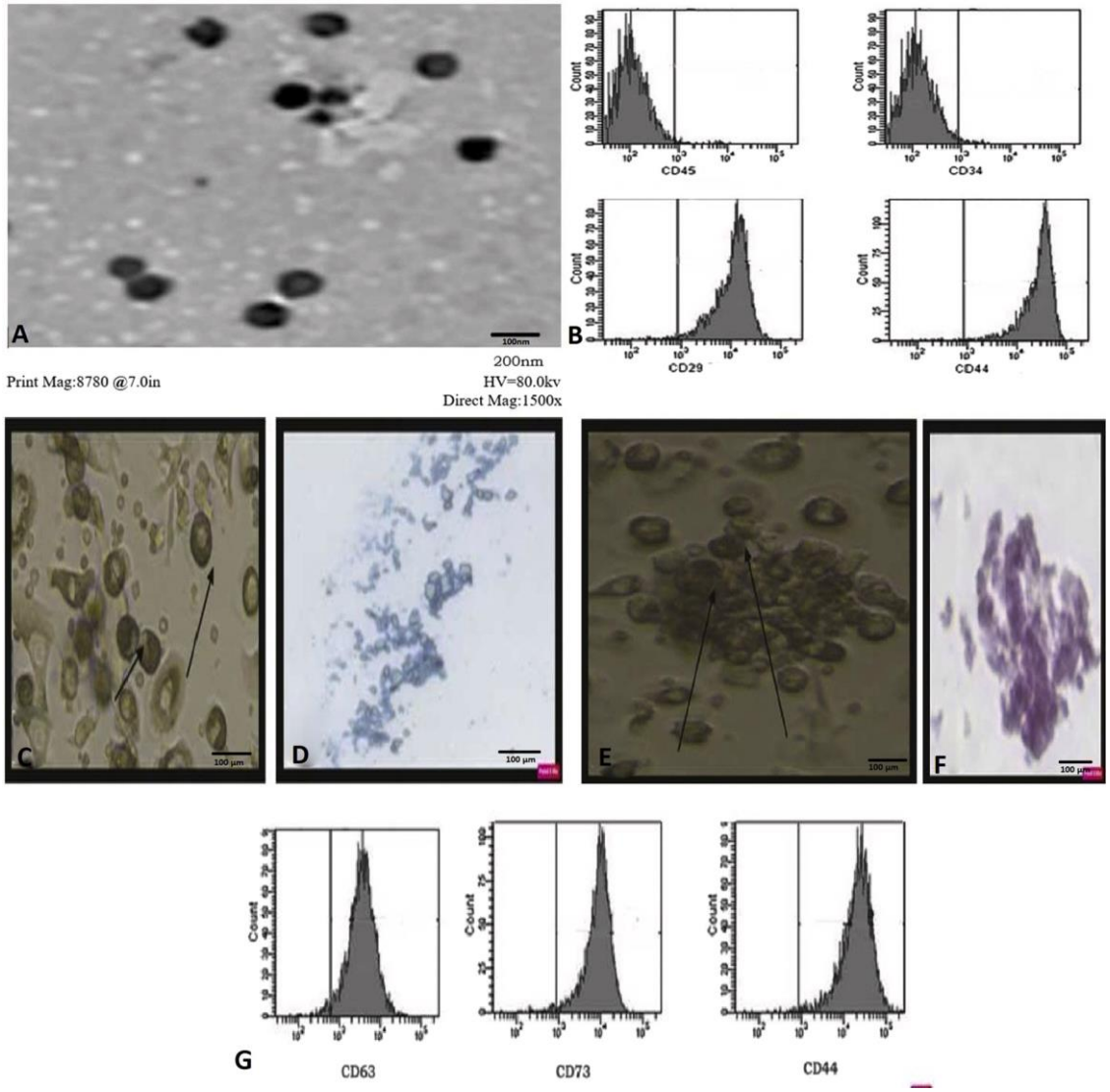

Fig. 1. A) TEM images of *Soy nano-isoflavone* with low and high magnification power. **B)** Flowcytometry showing positive expression of BMSCs markers (CD29, CD44) and negative expression of hematopoietic markers (CD34, CD45). BMSCs differentiated into chondrocytes. **C)** Arrows point to differentiated MSCs into chondrocytes. (X200). **D)** Differentiated MSCs into chondrocytes stained with Alcian Blue stain (X200). BMSCs differentiated into osteoblasts. **E)** Arrows point to differentiated MSCs into osteoblast (X200). **F)** Differentiated MSCs into osteoblasts stained with Alizarin red stain (X200). **G)** Flowcytometry showing positive expression of BMSCs-EXs markers (CD63, CD73, CD44).

2.12.2. Morphometric study

All cerebral cortex Immuno-stained sections from all groups were observed by light microscopy on high power field. The area percentages in astrocytes for GFAP positive immune-stained were estimated in ten images for each group. The number of astrocytes and microglia (stained using CD68 immunohistochemistry) was counted in 10 HPFs in each specimen (Hämäläinen et al., 2008). The number of cells were analyzed utilizing the computerized image analyzer software system (Leica Q500-MCO, Leica, Wetzlar, Germany) (Leica Universal Microscope at Histology Department, Faculty of Medicine, Cairo University). Light microscope with an×40 objective lens was used for measurement.

2.13. Statistical analysis

The Statistical Package of Social Studies programmer (SPSS) version 16.0.1 (SPSS Inc., Chicago IL, United States) was used. Information was obtainable as mean ± SD. Differences between groups were analyzed by t- test. Post-hoc testing was done by a Tukey test for multiple comparisons of the differences between the groups after applying ANOVA to detect differences. Statistical significances were considered at $p < 0.05$.

3. Result

3.1. Soy nano-isoflavone characterization

The average diameter of each particle was shown as 237.9 ± 2.8 nm and the width of 112.1 nm, whereas the PDI was 0.178 ± 0.001, confirming the uniform spreading of all particles in the formulation. The Saturation-solubility of the nano particles confirmed the accommodation ability of the particle to greater number of metabolites (MK-677.71 lg/mL, nattokinase 83.2 FU/mL, genistein 210.31 lg/mL, Isoflavones daidzein 179.21 lg/mL, and glycitein 79.91 lg/mL) in solution (Table 2).

3.2. Characterization of soy nano-isoflavones

Examination of the soy nano - isoflavone by transmission electron microscope (TEM) and scanning electron microscope (Fig. 1A), revealed rounded and ovoid in shape with good particle dispersion of soy nano-isoflavone.

3.3. Characterization of immunophenotyping of MSCs

Immunophenotyping was positive for monoclonal antibodies against CD29 and CD44, while antibodies against CD34 and CD45 were negative (Fig. 1B).

3.4. Adipogenic and osteogenic differentiation potential of MSCs

BMSCs differentiation, osteogenic and adipogenic ability was evaluated after cell disclosure to the basic osteogenic and adipogenic differentiation protocols for two to three weeks as previously described (Fig. 1C&D and E&F).

3.5. Characterization and homing of MSCs-EXs

BMSCs-EXs were identified by flowcytometry by using surface markers for CD73, CD44, and CD63 as (more than 90 % of MVs were positive) by flow cytometry analysis (Fig. 1G). Additionally, they were identified by electron microscope as ovoid structures (Fig. 2(A)), while homing of PKH26 fluorescent - labeled BMSCs- EXs was detected in brain tissue by fluorescent microscope in the treated groups of BMSCs-EXs both in vivo and in vitro as strong red fluorescence (Figs. 2(B)

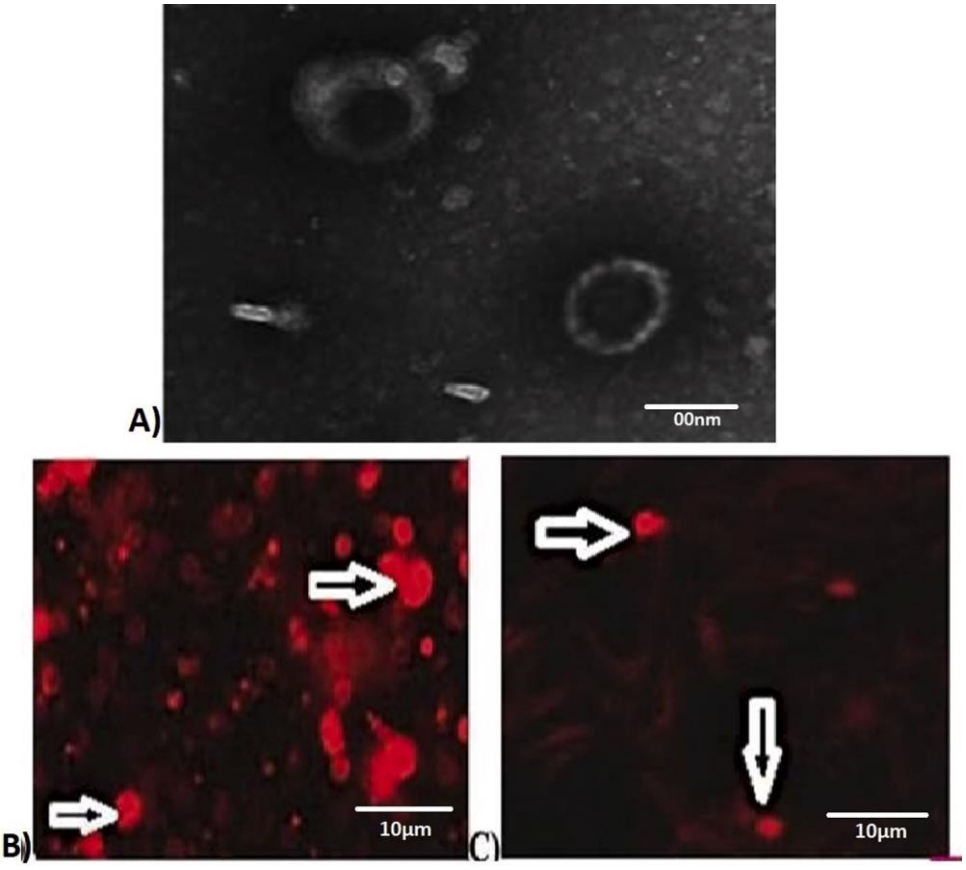

Fig. 2. A) Electron microscopy image of identified BMSCs-EXs using ultracentrifugation (arrow). Scale bar: 100 nm. Fig. 1(B) Labeling of BMSCs-EXs with a fluorescent dye PKH26 (in vitro), Fig. 1(C) homing of the labeled BMSCs-EXs by detecting PKH26 fluorescent dye in the brain tissue (in vivo).

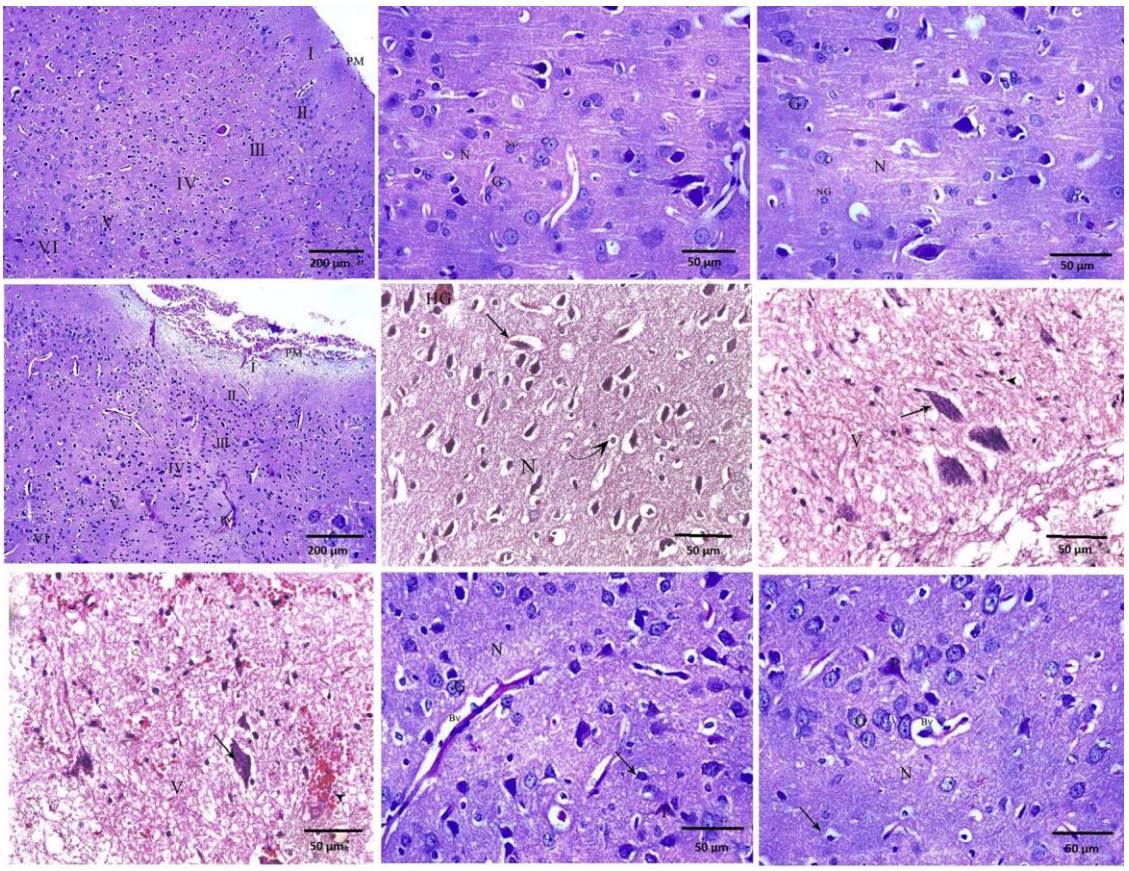

Fig. 3. A) A photomicrograph of section in the cerebral cortex of adult male albino rat of control group (Ia) showing the pia matter (PM) covers the outer molecular layer (I) followed by external granular layer (II), external pyramidal layer (III), inner granular layer (IV), inner pyramidal (V) and the polymorphic layer (VI) (H&E x100). **(B)** A photomicrograph of section in the cerebral cortex of adult male albino rat of control group (Ia) showing normal pyramidal cell (P) of multipolar shape with large, vesicular nucleus and basophilic cytoplasm. Granular cells (G) with large nuclei, major nucleolus, and small amount of cytoplasm. Also, neuroglia cells can be seen (NG). The pink stained background is the neuropil (N) (H&E x400). **(C)** A photomicrograph of section in the cerebral cortex of adult male albino rat of control group (Ib) showing normal multipolar shaped pyramidal cell (P) and rounded, vesicular nucleus with basophilic cytoplasm. Granular cells (G) can be seen with large nuclei, prominent nucleolus, and little cytoplasm. Also, neuroglia cells can be seen (NG). The pink stained background is the neuropil (N) (H&E x400). **(D)** A photomicrograph of section in the cerebral cortex of adult male albino rat of ND group II showing the pia matter (PM) which covered with extravasated blood. The outer molecular layer (I) followed by external granular layer (II), external pyramidal layer (III), inner granular layer (IV), inner pyramidal (V) and the polymorphic layer (VI) can be seen. Multiple dilated congested blood vessels (Bv) can be observed (H&E x100). **(E)** A photomicrograph of section in the cerebral cortex of adult male albino rat of ND group II showing that all pyramidal cells are shrunken, surrounded with empty spaces with loss of their processes and small darkly stained nuclei (arrow). Many apoptotic cells (curved arrow) can be observed. These cells are shrunken with pyknotic nuclei (darkly stained) and little acidophilic cytoplasm. Also, area of hemorrhage (HG) can be seen. Notice, the neuropil (N) appears vacuolated (H&E x400). **(F)** A photomicrograph of section in the cerebral cortex of adult male albino rat of ND group II showing that the pyramidal cells surrounded with halos and contain intracellular fibrillar neurofibrillary tangles (arrow) with vacuolated neuropils (V). Extravasated blood (arrowhead) can be seen (H&E x400). **(G)** A photomicrograph of section in the cerebral cortex of adult male albino rat of ND group II showing that the pyramidal cells surrounded with halos and contain intracellular fibrillar neurofibrillary tangles (arrow) with vacuolated neuropils (V). Extravasated blood (arrowhead) can be seen (H&E x400). **(H)** A photomicrograph of section in the cerebral cortex of adult male albino rat of treated group III showing marked improvement with the pyramidal cells (P) appear mostly as in control group. Few pyramidal cells appear shrunken and surrounded with haloes (arrow). Granular cells (G) with rounded open face nuclei are also seen. The pink stained background is the neuropil (N), but it is still slightly vacuolated. Dilated congested blood vessel (Bv) can be seen (H&E x400). **(I)** A photomicrograph of section in the cerebral cortex of adult male albino rat of treated group IV showing marked improvement with the pyramidal cells (P) appear mostly as in control group. Few pyramidal cells appear shrunken and surrounded with haloes (arrow). Granular cells (G) with rounded open face nuclei are also seen. The pink stained background is the neuropil (N) but it is still slightly vacuolated. Dilated congested blood vessel (Bv) can be seen (H&E x400). [x100 scale bar = 200 µm, x400 scale bar = 50 µm].

Table 3
Effect of MSCs-EX injection and Soy nano-isoflavone on neurodegenerative disorders-impaired learning and memory in rats evaluated by water maze.

Groups	Group I(control)	Group II (neurodegenerative)	Group III (isoflavone-treated)	Group IV (MSCs-treated)
Escape latency	14.5 ± 0.10	66.15 ± 0.25 [a]	17.62 ± 0.19 [a b]	19.42 ± 0.11 [a b]

Data a are expressed as mean ± SE. [a] significant Vs control group and [b] significant Vs diseased group ($p < 0.05$).
-Group I: control group. Group II: neurodegenerative disorders group. Group III: Soy protein nano-isoflavone extract treated group. Group IV: MSCs-EXs treated group.

Table 4
Effect of MSCs or Nano soybean treatment on oxidative stress markers cerebral tissue.

Parameters/groups	Group I (control)	Group II (neurodegenerative)	Group III (isoflavone-treated)	Group IV (MSCs-treated)
SOD (mg/g)	82.41 ± 0.47	65.26 ± 1.23 [a]	74.21 ± 1.26 [a b]	77.31 ± 0.13 [a b]
MDA (nmol/g)	154.17 ± 1.11	309.54 ± 1.07[a]	270.12 ± 2.78 [a b]	225.32 ± 0.47 [a b]
GSH (mg/g)	28.36 ± 1.57	24.19 ± 0.95 [a]	26.47 ± 0.61 [a b]	27.30 ± 1.99 [a b]
CAT (U/g)	51.28 ± 3.94	39.89 ± 1.29[a]	47.27 ± 1.69 [a b]	49.08 ± 0.59 [a b]

-MDA, malondialdehyde; GSH, reduced glutathione; CAT, catalase.
Data are expressed as mean ± SE. [a] significant Vs control group and [b] significant Vs diseased group ($p < 0.05$).
-Group I: control group. Group II: neurodegenerative disorders group. Group III: Soy protein nano-isoflavone extract treated group. Group IV: MSCs-EXs treated group.

and 3 (C)).

3.6. Morris water maze test results

Neurodegenerative disorders group (ND) showed higher escape latencies (time taken to find platform) of around 66 s than the control group ($P < 0.05$), which showed 14 s escape latency, and this means impairment in their memory in diseased animals, while in the control animals they were able to locate the platform faster. BMSCs-EXs injected and soy nano-isoflavone supplemented groups exhibited a significant decrease in escape latencies' period in comparison to ND animals ($p < 0.05$). There was a significant improvement in the ability to find out the hidden platform inside the water pool (Table 3).

3.7. Oxidative markers results

BMSCs-EXs injection and soy nano-isoflavone supplementation reduces oxidative damage in experimental induced neurodegenerative disorders. As compared with the control group, ND group showed significantly decreased SOD and GSH activities ($p < 0.05$). Soy nano-isoflavone treatment significantly increased the levels of SOD and GSH in comparison to ND group. MSCs-EXs treatment exhibited more significant elevation ($p < 0.001$) in SOD and GSH in comparison to ND group. MDA level was significantly increased ($p < 0.05$) in ND group as compared to the control group. Soy nano-isoflavone and BMSCs-EXs treatment led to a considerable decrease ($p < 0.05$, $p < 0.001$ respectively) of MDA level as compared to the ND group. CAT levels showed a significant decrease in ND group as compared to the control group ($p < 0.001$). Soy nano-isoflavone and BMSCs-EXs treatment led to significant increases ($p < 0.05$, $p < 0.001$respectively) in CAT levels in comparison to the ND group (Table 4).

3.8. Quantitative gene expression results

All results of TNF-α, iNOS, and GAPDH gene expression for all groups are represented in Table 5. In ND group, there was a significant increase in the relative gene expression levels of TNF-α and iNOS in comparison to the control group. Treatment with either soy nano-isoflavones or BMSCs-EXs led to a significant decrease in TNF-α and iNOS gene expression levels as compared with ND group ($p < 0.001$).

Table 5
Tumor necrosis factor (TNF α), inducible a nitric oxide synthase (i NOS), and Glyceraldehyde 3- phosphate a dehydrogenase (GAPDH) genes expression in all groups. Results are presented as Mean ± SD.

Parameters/ groups	Group I (control)	Group II (neurodegenerative)	Group III (Isoflavone-treated)	Group IV (MSCs-treated)
TNF-α	0.55 ± 0.47	0.76 ± 1.21 [a]	0.59 ± 0.36 [a b]	0.50 ± 0.12 [a b]
iNOS	0.79 ± 0.94	1.89 ± 0.35 [a]	0.81 ± 0.15 [a b]	0.80 ± 0.12 [a b]

Data a are expressed as mean ± SE. [a] significant Vs control group and [b] significant Vs diseased group ($p < 0.05$).
-Group I: control group. Group II: neurodegenerative disorders group. Group III: Soy protein nano-isoflavone extract treated group. Group IV: MSCs-EXs treated group.

3.9. Histological result

3.9.1. H&E stain

Examination of slides of rat cerebral cortex of the frontal lobe from the control group showed normal characteristic histological features of the cerebral cortex layers as nerve cell groups that are organized in six layers enclosed by pia mater, the molecular layer (M), outer granular layer(G), outer pyramidal layer(P), inner granular layer, the inner pyramidal, and the polymorphic layers (PO). The molecular layer(M) was wide, containing a dense plexus of nerve fibers with little cells. On the other hand, external granular (G) and external pyramidal (P) comprised many granular cells (G) & pyramidal cells (P). The internal granular and internal pyramidal revealed little granular cells and pyramidal cells. These layers were ill defined from each other. Higher magnification of the cortex showed many cells; the pyramidal cells pyramidal cells had a multipolar shape and basophilic cytoplasm with long dendrites, while rounded granular cells exhibited large vesicular nuclei and pronounced nucleoli with little cytoplasm. In between neurons there were blood vessels and neuroglial cells. The ground material among neuronal cells is normally contained neuropil that appeared as an eosinophilic homogenous background (Fig. 3A, B, C, D and E).

In ND disease group (group II), microscopic examination showed six layers of the cerebral cortex, but the pia mater covered with extravasated blood. All pyramidal cells surrounded by haloes and appeared shrunken, lost processes with darkly stained pyknotic nuclei. Some pyramidal cells contained intracellular fibrillar neurofibrillary tangles. Many apoptotic cells could be observed. These cells were shrunken with pyknotic nuclei (darkly stained) and little acidophilic cytoplasm. There was also extensive neuropil vacuolization. Dilated congested blood vessels and extravasated blood were seen within the neuropil. Additionally, the area of hemorrhage can be detected. The histological structure of the treated groups with soy protein nano- isoflavone extract and MSCs-EXs (III and IV) was more or less similar to that in group control group as showed normal multiple pyramidal cells with decreased perineuronal haloes. However, few neuronal cells appeared shrunken and surrounded by haloes (Fig. 3F, H, and I). Additionally, the neuropil was still slightly vacuolated with dilated congested blood vessels.

3.9.1.1. Silver stain. Silver-stained sections of the control group showed pyramidal cells, neurofibrils, and the intercellular area (neuropil) in between. Silver-stained sections of ND disease group II showed neuritic argentophilic plaques among the cells and accumulated fibrils and encircled by a clear halo. Also, showed intracellular neurofibrillary tangles and vacuolated neuropils. Examination of silver-stained sections of groups III and IV showed that the histological structure appeared nearly as the control group (Fig. 4).

3.9.1.2. Immunohistochemical result. Detection of astrocytes by using glial fibillary acidic protein (GFAP) immunostaining showed a positive

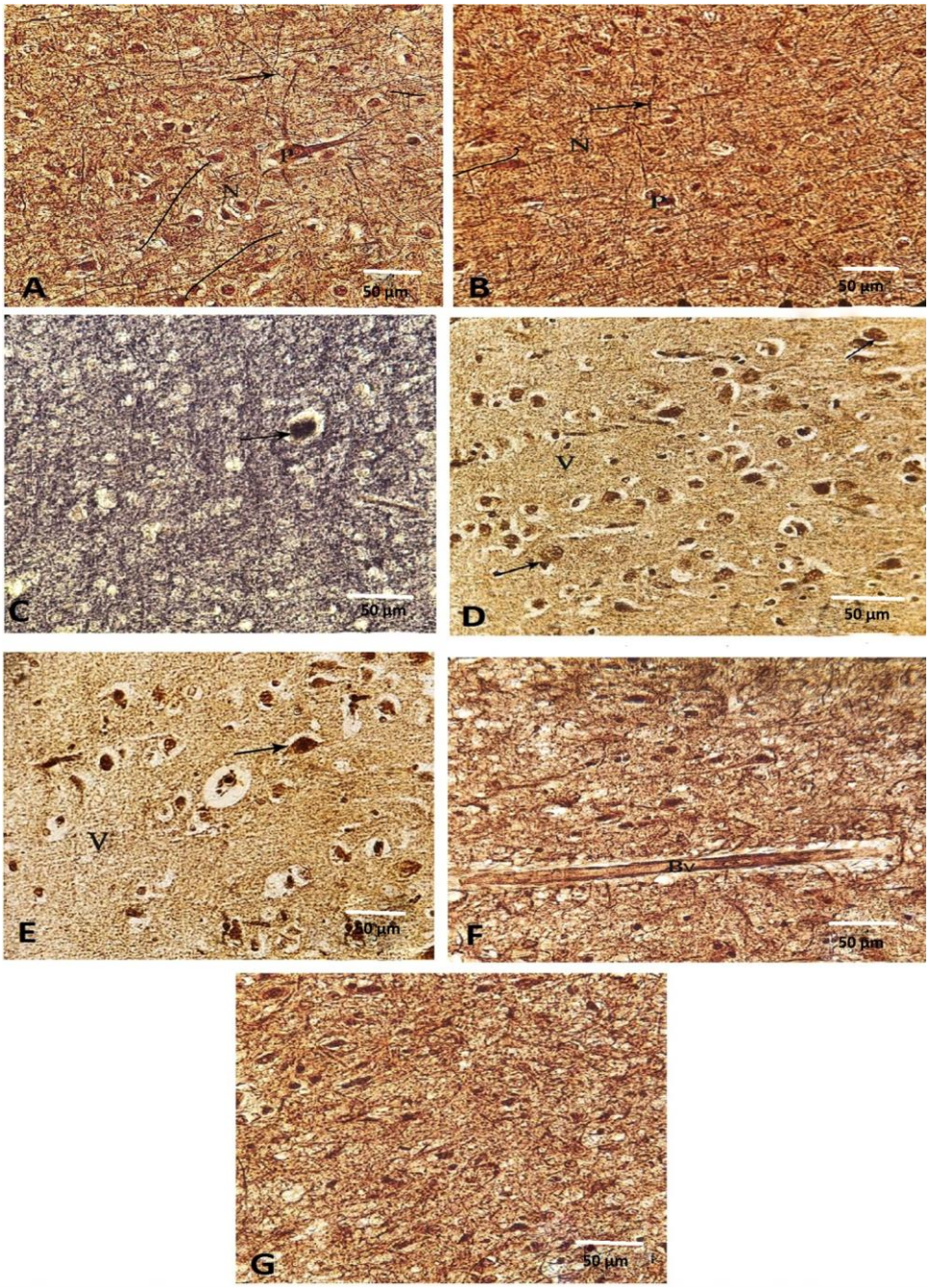

Fig. 4. (A) A photomicrograph of section in the cerebral cortex of adult male albino rat of control group (Ia) showing multiple neurons (P), neuropil in between (N) and neurofibrilles (arrow). **(B)** A photomicrograph of section in the cerebral cortex of adult male albino rat of control group (Ib) showing multiple neurons (P), neuropil in between (N) and neurofibrilles (arrow). **(C)** A photomicrograph of section in the cerebral cortex of adult male albino rat of ND group II showing silver-positive neuritic plaques (arrow) surrounded by a clear halo. **(D)** A photomicrograph of section in the cerebral cortex of adult male albino rat of ND group II showing argentophilic neurofibrillary tangles within the cytoplasm of nerve cells which surrounded by halos (arrows) and vacuolated neuropil (V). **(E)** A photomicrograph of section in the cerebral cortex of adult male albino rat of ND group II showing argentophilic neurofibrillary tangles within the cytoplasm of nerve cells which surrounded by halos (arrow) and vacuolated neuropil (V). **(F)** A photomicrograph of section in the cerebral cortex of adult male albino rat of treated group III showing that the histological picture is the same as the control group but dilated congested blood vessel (Bv) can be seen. **(G)** A photomicrograph of section in the cerebral cortex of adult male albino rat of treated group IV showing that the histological picture is the same as the control group (Silver stain x400, scale bar = 50 µm).

cytoplasmic reaction in the control group (Ia, Ib). In ND disease group II, there was an apparent marked increase in the immunostaining with rise in the number of immune-reactive astrocytes for GFAP matched with the control group. The treated rats (groups III and IV) showed diminished in GFAP immunostaining cells in addition to decreased in the number of immune-reactive visible astrocytes compared with the control group (Fig. 5). There were few positive stained cells in the control group of microglia/macrophage staining using CD68 immunohistochemistry. Here was a significant rise in the immunostaining and number of activated microglia/macrophages which were positively dyed with CD68 in ND disease group II. In the groups treated with Soy protein nano-isoflavone extract and BMSCs-EXs (III and IV), there was few positive microglia/macrophages immunostaining using CD68 (Fig. 6) compared to the control group.

3.9.1.3. Morphometric result. The means area % of a positive GFAP immunoreactive stain in astrocytes for all groups were represented in (Table 6). In ND disease group showed a significant increase in area % for GFAP in positive staining ($P < 0.001$) in relation to control, and in both groups treated by soy protein nano-isoflavone extract and BMSCs-EXs showed a decrease in area % for GFAP in positive staining.

In ND disease group revealed a very significant elevated in the number of astrocytes contrasted with control rats. In both groups treated by soy protein nano-isoflavone extract and BMSCs-EXs showed a significant decrease in the number of astrocytes and revealed no significant differences when compared with the control group (Table 6). In ND disease group showed a highly significant increase in the number of microglia stained using CD68 immunohistochemistry compared with control rats, while in soy protein nano-isoflavone extract and BMSCs-EXs treated groups revealed no significant differences when compared with the control group (Table 6).

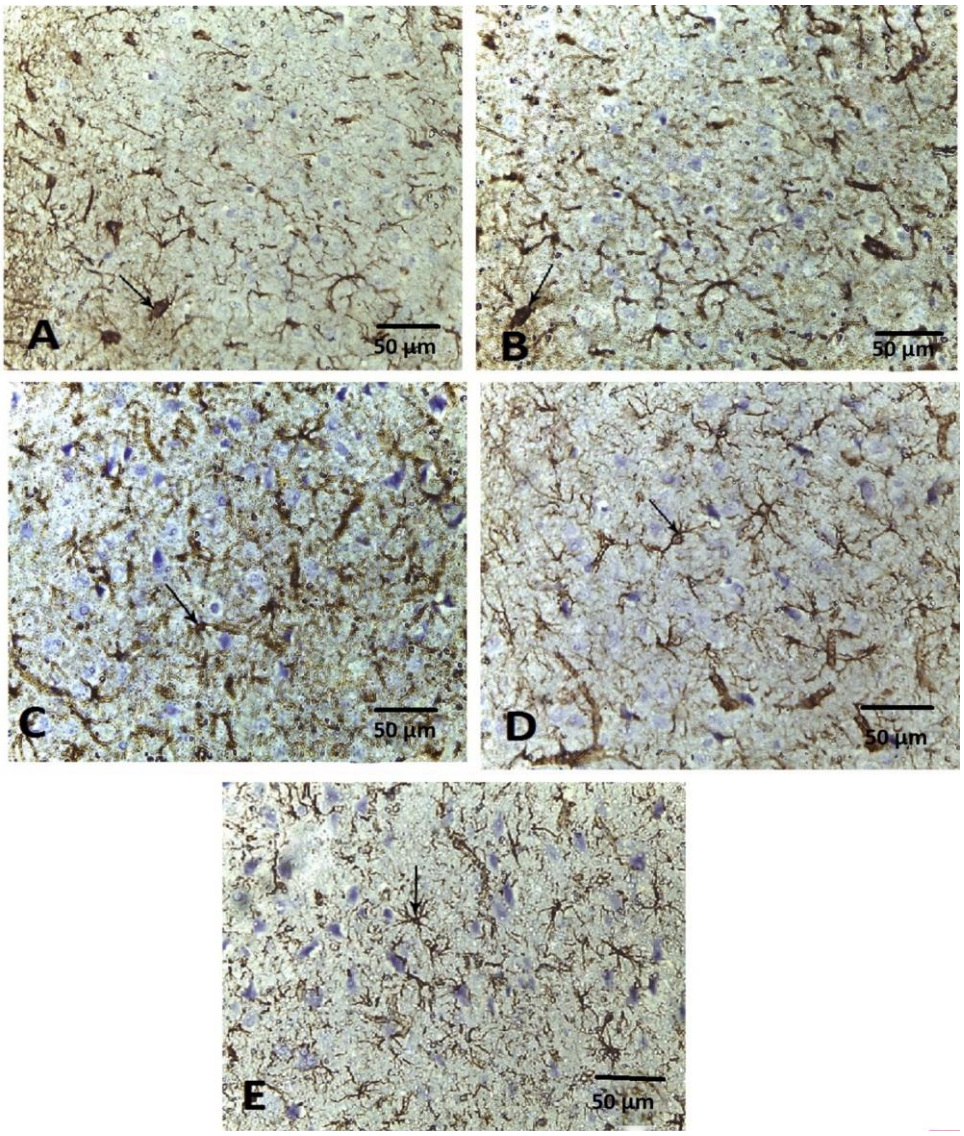

Fig. 5. A) A photomicrograph of section in the cerebral cortex of adult male albino rat of control group (Ia) showing positive cytoplasmic reaction for GFAP immunostaining for astrocytes(arrow). A photomicrograph of section in the cerebral cortex of adult male albino rat of control group (Ib) showing positive cytoplasmic reaction for GFAP immunostaining for astrocytes (arrow). **(C)** A photomicrograph of section in the cerebral cortex of adult male albino rat of ND group II showing apparent marked increase in the cytoplasmic reaction for GFAP immunostaining for astrocytes (arrow). **(D)** A photomicrograph of section in the cerebral cortex of adult male albino rat of treated group III showing some immunostained positive cells (arrow) for GFAP immunostaining for astrocytes. **(E)** A photomicrograph of section in the cerebral cortex of adult male albino rat of treated group IV showing some immunostained positive cells (arrow) for GFAP immunostaining for astrocytes. (Avidin biotin peroxidase stain with Hx counter stain x400, scale bar = 50 µm).

4. Discussion

Degeneration of the brain tissue is related to cell apoptosis, axonal failure to regenerate, and demyelination, that lead to abnormal structure and function of neurons. All these conditions may be due to genetic or acquired causes. These illnesses affect the normal performance of the CNS and result in the continuing decrease or even the extensive loss of motor, sensory, and cognitive work. Examples, Alzheimer's disease (AD), multiple sclerosis (MS), and Parkinson's disease (PD) (Hussain et al., 2018). D-galactose is present usually in the human body as one of the reducing sugars. In normal blood levels, D-galactose is transformed into glucose. Whereas, at elevated blood levels, it is subjected to oxidation and conversion into H2O2 and aldehydes. Injection of D-galactose into the rodent for 6–10 weeks lead to progressive deterioration of cognitive function and increased generation of free oxygen radicals in brain tissue. Damage induced by free oxygen species lead to neuronal degeneration (El-Safti et al., 2017). In the present study, the cerebral cortex of neurodegenerative disorders - induced model group showed that all pyramidal cells surrounded by haloes and appeared shrunken, lost their processes with darkly stained pyknotic nuclei. Some pyramidal cells contained intracellular fibrillar neurofibrillary tangles. Many apoptotic cells could be observed. These cells were shrunken with pyknotic nuclei and little acidophilic cytoplasm. There was also extensive neuropil vacuolization. Dilated congested blood vessels and extravasated blood were seen within the neuropil. Neurofibrillary tangles were detected as soluble twisted fibers inside brain tissues of ND group. The neurofibrillary tangles consist of a protein called tau, which function as microtubule associated proteins. In ND disease, tau proteins undergo chemical changes and hyperphosphorylation. Then tau proteins combine by microtubules, producing neurofibrillary tangles that lead to disorders to destruction of the neuronal transportation system in the brain tissue (Duncan and Valenzuela, 2017). In the current study, amyloid plaques were identified in the silver-stained sections between neuronal cells, accumulating fibrils surrounded by a clear halo, intracellular fibrillar neurofibrillary tangles and vacuolated neuropils.

Finding of amyloid plaques in ND induced model rats are approved with other findings stated by several studies which showed that the accumulation of amyloid plaques(ap) is one of the features of ND disease among neuronal cells of the brain. β-Amyloid (ap) is a fragment of protein as result of trimming of an amyloid protein precursor, these amyloid proteins normally remain exposed to proteolysis then taken away. The amyloid proteins are collected and form insoluble hard plaques in ND disease, that are the toxic and lead to neuronal dysfunction, impaired calcium homeostasis, and stimulating cell apoptosis (Minett et al., 2016). Seriously, so NDs diseases characterized by presence of an atypical formation of proteins in the tissue of brain and the common

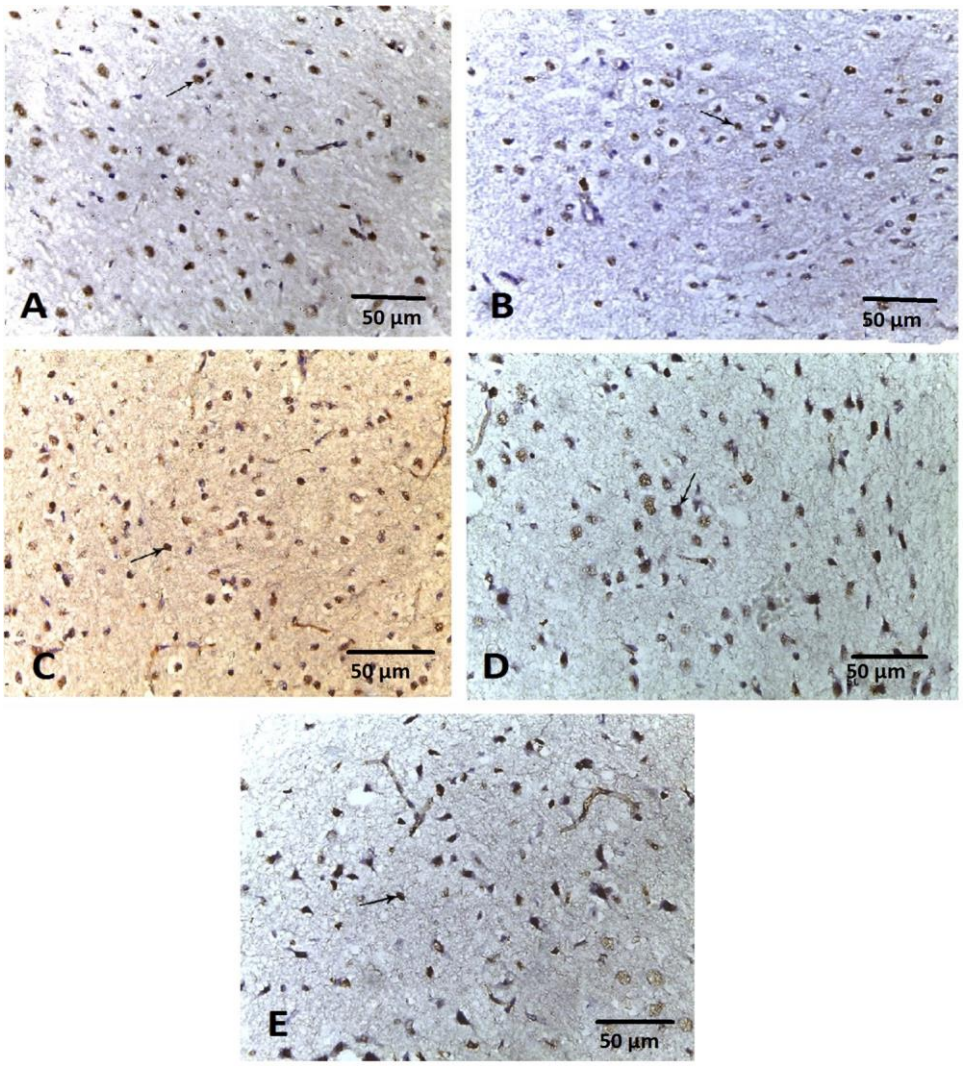

Fig. 6. A) a photomicrograph of section in the cerebral cortex of adult male albino rat of control group (Ia) showing few immunostained positive cells (arrow) for CD68. **(B)** a photomicrograph of section in the cerebral cortex of adult male albino rat of control group (Ib) showing few immunostained positive cells (arrow) for CD68. **(C)** a photomicrograph of section in the cerebral cortex of adult male albino rat of Alzheimer group II showing apparent increase in immunostained positive cells (arrow) for CD68. **(D)** a photomicrograph of section in the cerebral cortex of adult male albino rat of treated group III showing few immunostained positive cells (arrow) for CD68. **(E)** a photomicrograph of section in the cerebral cortex of adult male albino rat of treated group IV showing few immunostained positive cells (arrow) for CD68. (Avidin biotin peroxidase stain with Hx counter stain x400, scale bar = 50 µm).

Table 6
Mean ± SD of Area % for GFAP expression, astrocytes, and microglia (staining using CD68 immunohistochemistry) counts in different experimental groups.

Parameters/groups	Group I (control)	Group II (neurodegenerative)	Group III (isoflavone-treated)	Group IV (MSCs-treated)
astrocytes	19.71 ± 1.62	38.58 ± 1.381[a]	28.01 ± 2.178 [a b]	28.31 ± 1.561 [a b]
microglia staining using CD68 immunohistochemistry	4.96 ± 1.015	9.639 ± 0.967 [a]	5.10 ± 0.09 [a b]	4.118 ± 0.032 [a b]
Area % for GFAP expression	1.3 ± 0.03	7.9 ± 0.01[a]	4.5 ± 0.02[ab]	2.3 ± 0.04[ab]

Data are expressed as mean ± SE. [a] significant Vs control group and [b] significant Vs diseased group ($p < 0.05$).
-Group I: control group. Group II: neurodegenerative disorders group. Group III: Soy protein nano-isoflavone extract treated group. Group IV: MSCs-EXs treated group.

examples of these proteins are β-amyloid in AD, ubiquitinated proteins in amyotrophic lateral sclerosis (Blokhuis et al., 2013), misfolded Huntington protein in HD, and presence of Tau and β-amyloid in MS plaques (David and Tayebi, 2014). Proof recommends that the presence of misfolded protein significantly related to the advancement of disease (David and Tayebi, 2014). The brain damage was explained due to an increase in oXidative stress that gives the idea of the pathogenesis of neurodegenerative diseases. OXidative stress- caused damage led to neuronal degeneration and harms the normal function of astrocytes. Astrocytes, which are plentiful glial cells that share in neuralelectrical activity and blood brain barrier formation. As a result of the disease, astrocytes become activated to mediate neuronal protection. Additionally, stimulated astrocytes have antioXidant activity through increasing in glutathione (GSH) levels and decreasing in neurotoXin release.

Impaired functions of astrocytes are present in different ages such as in some neurodegenerative such as multiple sclerosis, Parkinson's disease, and Alzheimer disease. Astrocytes end feet share in the blood- brain barrier, which have essential roles in maintaining the homeostasis of the brain microenvironment. Therefore, astrocyte's function is the first line of defense in response to free oXygen radicals in the blood stream. Thus, astrocytes have decreased antioXidant capability, generating nitric oXide (NO) by upregulation of iNOS gene expression (Hatters, 2008). In the present study, decreased GSH levels, increased iNOS levels confirm this view. Additionally, the immunohistochemical results of glial fibillary acidic protein (GFAP) for detection of astrocytes activity showed an apparent marked increase in the immunostaining including elevates in the number of immune-reactive astrocytes for GFAP matched to the control group. Microglia are resident tissue macrophages of the central

nervous system and play essential functions in immune surveillance inside the brain. Microglia reacts to neuronal or synaptic damage and abnormal accumulation of tau proteins, fundamental features of Alzheimer disease (Chistiakov et al., 2017). It was noticed that the inflammatory processes could play important roles in the pathogenesis of neurodegenerative disease. The presence of stimulated microglia with amyloid plaques in neurogenerative disease induces cytokines such as interleukin-1βaa (IL-1β), tumor necrosis factor-α (TNF-α), and NO40. The transmembrane glycoprotein proteins conveyed by monocytes and tissue macrophages for phagocytic activity are CDs68. It is present in phagocytic lysosomes within microglia. CD68 is an immune chemical marker of macrophages and other mononuclear phagocytes (Xi et al., 2013; Gallagher et al., 2015; Waller et al., 2019). In the current study, there was a significant rise in the immune staining by CD68 and the number of stimulated microglia/ macrophages in ND group. This was supported by a study conducted by (Xi et al., 2013) who stated that the association of CD68 with dementia, poor cognitive function is strong. In the study of macrophage indicators in postmortem human brain tissues from normal persons and from with Alzheimer disease, there was an upregulation of CD68 in neurodegenerative disorders group in comparison to the control brain tissues (Xi et al., 2014). These findings support our results of increasedCD68 expression. Morris water maze task was intended to examine the rat's capability to determine the specific locations in a wide area. This test is widely used in neurobiological studies and in the characterization of cognitive decline in aged rats (Reza-Zaldivar et al., 2019; Lepeta et al., 2016b). The ND group in this study showed advanced escape latencies (time taken to find platform) of around 66 s than the control group, which showed 14 s escape latency, and this means a disturbance in their memory in ND animals, while in the control animals they were able to locate the platform faster. Up to our knowledge, there is a deficiency of effective drugs that target the pathophysiological insult in ND. Polyphenols are micronutrients that are found in most plants, fruits, and vegetables. Polyphenols include flavonoids, non-flavonoids, phenolic acids, and phenolic amines. Soybeans are rich sources of isoflavones which are linked to flavonoid polyphenols. Several studies have evidenced the neuroprotective effects of isoflavones against cognitive impairment induced by amyloid beta peptide (Qu and Zhang, 2017; Harris et al., 2018; Donders et al., 2018). These findings agree with results of the present study which showed that the use of soy nano-isoflavones and MSCs-EXs exerted significant beneficial effects against ND induced histopathological changes. In nano-isoflavones and in BMSCs-EXs treated groups, neuronal cells within the neurofiberlls appeared nearly normal. Results of BMSCs-EXs treated group in our study agree with previous findings (Nakano et al., 2016; Yang et al., 2017a), which proved that BMSCs-EXs significantly increased neurogenesis in the brain tissue and significantly decreased amyloid beta- induced cognitive impairment. MSCs increase anti-inflammatory cytokines that can stimulate neuritic growth, neuro- degeneration, and neurologic recovery (Yang et al., 2017b; Drom- melschmidt et al., 2017). BMSCs mediate their functions through the paracrine activity and not by direct cell regeneration (Phinney and Pittenger, 2017). Further studies confirmed that exosomes mediate the paracrine activities of BMSCs (TeiXeira et al., 2019). As regards oXi- dant/antioXidant markers, results of the present study showed that the use of soy nano-isoflavones and BMSCs-EXs led to a significant increase in antioXidant parameters: SOD, CAT, GSH as well as a significant decrease in oXidative stress markers: MDA and iNOS. These findings could be explained by the fact that nano-isoflavone exerts significant antioXidant effects with induction of glutathione peroXidase and in- crease in glutathione levels (Falcão et al., 2019). Other studies noticed similar findings. MSCs exert significant antioXidant effects in ND as well as other diseases (da Costa Gonçalves et al., 2017). da Costa Gonçalves et al. reported that systemic infusion of MSCs in a murine model of co- litis led to significant antioXidant effect by preventing the impairment in Glutathione levels and SOD enzyme activity. Furthermore Cui et al. (2017, 2018) found that umbilical cord mesenchymal stem cells (hUC-MSCs) significantly improved cognitive impairment in a murine model of neurodegenerative disorder. The authors stated that hUC-MSCs significantly decrease the oXidative stress in the neuronal tissue of ND mice by lowering the levels of malondialdehyde (MDA), increasing the action of nitric oXide synthase (nNOS) and superoXide dismutase (SOD). Similar results were reported using MSCs-EXs in Alzheimer disease (Elia et al., 2019; Cui et al., 2018). All these findings coincided with our results that showed significant improvement in oXidant/antioXidant balance in MSCs- EXs treated rat group. In conclusion, the use of either BMSCs-EXs or nano-isoflavones in the experimental model of neurodegenerative disorders exhibited significant amelioration of the neurological damage, significant restoration of the number of neurons, significant improvement in the oXidant/antioXidant balance and lowering of inflammatory cytokine.

Author contributions

Eman Faruk: searching the data and doing the histopathological techniques sections. Amal: writing the paper. Rehab AbdAllah Hasan: doing the statistical method. Neama Mahmoud: doing the biochemical analysis. Hanan Foud: preparing the gene for analysis.

Ethical approval

Approval has been obtained from the Local Ethical Committee for the experimental use of laboratory animals. Faculty of Medicine for Girls, Al-Azhar University, Cairo, Egypt (Approval Number IORG0010305).

Funding source

No funds were received by authors to do their research.

Availability of supporting data

Available on request.

Declaration of Competing Interest

The authors report no declarations of interest.

Acknowledgments

The authors would like to thank Dr. Mohammed A.S. Abourehab, Associate Professor of Pharmaceutics, Faculty of Pharmacy, Minia University, Minia, Egypt, who prepared the Isoflavones and provided them as a generous gift.

References

Ali, T., Badshah, H., Kim, T.H., Kim, M.O., 2015. Melatonin attenuates D-galactose-induced memory impairment, neuroinflammation and neurodegeneration via RAGE/NF- KB/JNK signaling pathway in aging mouse model. J. Pineal Res. 58, 71–85. https://doi.org/10.1111/jpi.12194.

Baghaei, K., Hashemi, S.M., Tokhanbigli, S., Asadi Rad, A., Assadzadeh-Aghdaei, H., Sharifian, A., Zali, M.R., 2017. Isolation, differentiation, and characterization of mesenchymal stem cells from human bone marrow. Gastroenterol. Hepatol. Bed Bench 10, 208–213.

Bancroft, J.D., Layton, C., 2013. The hematoXylin and eosin. In: Suvarna, S.K., Layton, C., Bancroft, J.D. (Eds.), Theory & Practice of Histological Techniques, 7th ed. Churchill Livingstone of El Sevier, Philadelphia, pp. 172–214. Ch. 10 and 11.

Bhatt, P.C., Pathak, S., Kumar, V., Panda, B.P., 2018. Attenuation of neurobehavioral and neurochemical abnormalities in animal model of cognitive deficits of Alzheimer's disease by fermented soy bean nanonutraceutical. Inflammopharmacology 26 (Feb (1)), 105–118. https://doi.org/10.1007/s10787-017-0381-9.

Blokhuis, A.M., Groen, E.J.N., Koppers, M., van den Berg, L.H., Pasterkamp, R.J., 2013. Protein aggregation in amyotrophic lateral sclerosis. Acta Neuropathol. 125, 777–794. https://doi.org/10.1007/s00401-013-1125-6 [PMC free article] [PubMed] [CrossRef] [Google Scholar].

Boiko, D.A., Pentsak, E.O., Cherepanova, V.A., Ananikov, V.P., 2020. Electron microscopy dataset for the recognition of nanoscale ordering effects and location of nanoparticles. Sci. Data 7 (Mar (1)), 1–8.
Chernyshev, V.S., Chuprov-Netochin, R.N., Tsydenzhapova, E., Svirshchevskaya, E.V., Poltavtseva, R.A., Merdalimova, A., Yashchenok, A., Keshelava, A., Sorokin, K., Keshelava, V., Sukhikh, G.T., 2021. Asymmetric depth-filtration-a versatile and scalable approach for isolation and purification of extracellular vesicles. bioRxiv (Jan).
Chistiakov, D.A., Killingsworth, M.C., Myasoedova, V.A., Orekhov, A.N., Bobryshev, Y. V., 2017. CD68/macrosialin: not just a histochemical marker. Lab. Investig. 97 (Jan (1)), 4–13, 2017.
Cui, Y., Ma, S., Zhang, C., Cao, W., Liu, M., Li, D., Lv, P., Xing, Q., Qu, R., Yao, N., Yang, B., Guan, F., 2017. Human umbilical cord mesenchymal stem cells transplantation improves cognitive function in Alzheimer's disease mice by decreasing oxidative stress and promoting hippocampal neurogenesis. Behav. Brain Res. 320 (Mar), 291–301. https://doi.org/10.1016/j.bbr.2016.12.021, 2017.
Cui, G.H., Wu, J., Mou, F.F., Xie, W.H., Wang, F.B., Wang, Q.L., Fang, J., Xu, Y.W., Dong, Y.R., Liu, J.R., Guo, H.D., 2018. Exosomes derived from hypoxia-preconditioned mesenchymal stromal cells ameliorate cognitive decline by rescuing synaptic dysfunction and regulating inflammatory responses in APP/PS1 mice. FASEB J. 32 (Feb (2)), 654–668. https://doi.org/10.1096/fj.201700600R, 2018.
Cui, G.H., Guo, H.D., Li, H., Zhai, Y., Gong, Z.B., Wu, J., Liu, J.S., Dong, Y.R., Hou, S.X., Liu, J.R., 2019. RVG modified exosomes derived from mesenchymal stem cells rescue memory deficits by regulating inflammatory responses in a mouse model of Alzheimer's disease. Immun. Ageing (10). https://doi.org/10.1186/s12979-019-0150-0152. May 16.
da Costa Gonçalves, F., Grings, M., Nunes, N.S., Pinto, F.O., Garcez, T.N., Visioli, F., Leipnitz, G., Paz, A.H., 2017. Antioxidant properties of mesenchymal stem cells against oxidative stress in a murine model of colitis. Biotechnol. Lett. 39 (Apr (4)), 613–622. https://doi.org/10.1007/s10529-016-2272-3, 2017.
David, M.A., Tayebi, M., 2014. Detection of protein aggregates in brain and cerebrospinal fluid derived from multiple sclerosis patients. Front. Neurol. 5, 251. https://doi.org/10.3389/fneur.2014.00251.
Devi, K.P., Shanmuganathan, B., Manayi, A., Nabavi, S.F., Nabavi, S.M., 2017. Molecular and therapeutic targets of genistein in Alzheimer's disease. Mol. Neurobiol. 54 (Nov (9)), 7028–7041. https://doi.org/10.1007/s12035-016-0215-6.
Donders, R., Bogie, J.F.J., Ravanidis, S., Gervois, P., Vanheusden, M., Marée, R., Schrynemackers, M., Smeets, H.J.M., Pinxteren, J., Gijbels, K., Walbers, S., Mays, R. W., Deans, R., Van Den Bosch, L., Stinissen, P., Lambrichts, I., Gyselaers, W., Hellings, N., 2018. Human Wharton's Jelly-derived stem cells display a distinct immunomodulatory and proregenerative transcriptional signature compared to bone marrow-derived stem cells. Stem Cells Dev. 27, 65–84. https://doi.org/10.1089/scd.2017.0029, 2018.
Drommelschmidt, K., Serdar, M., Bendix, I., Herz, J., Bertling, F., Prager, S., Keller, M., Ludwig, A.K., Duhan, V., Radtke, S., de Miroschedji, K., Horn, P.A., van de Looij, Y., Giebel, B., Felderhoff-Müser, U., 2017. Mesenchymal stem cell-derived extracellular vesicles ameliorate inflammation-induced preterm brain injury. Brain Behav. Immun. 60, 220–232 (2017) [PubMed] [Google Scholar].
Duncan, T., Valenzuela, M., 2017. Alzheimer's disease, dementia, and stem cell therapy. Stem Cell Res. Ther. 8 (Dec (1)), 111.
Elia, C.A., Losurdo, M., Malosio, M.L., Coco, S., 2019. Extracellular vesicles from mesenchymal stem cells exert pleiotropic effects on Amyloid-β, inflammation, and regeneration: a spark of hope for Alzheimer's disease from tiny structures? Bioessays 41 (Apr (4)), e1800199. https://doi.org/10.1002/bies.201800199, 2019.
El-Safti, F.E., El-Kholoy, W.B., El-Mehi, A.E., Selima, R.R., 2017. A comparative study on the effect of aging on the hippocampal CA1 area of male albino rat. Menoufia Med. J. 30 (4), 1079, 1.
Falcão, H.G., Silva, M.B.R., de Camargo, A.C., Shahidi, F., Franchin, M., Rosalen, P.L., Alencar, S.M., Kurozawa, L.E., Ida, E.I., 2019. Optimizing the potential bioactivity of isoflavones from soybeans via ultrasound pretreatment: antioxidant potential and NF-κB activation, 2018 J. Food Biochem. 43 (Nov (11)), e13018. https://doi.org/10.1111/jfbc.13018.
Faruk, E.M., El-desoky, R.E., Al-Shazly, A.M., Taha, N.M., 2018. Does exosomes derived bone marrow mesenchymal stem cells restore ovarian function by promoting stem cell survival on experimentally induced polycystic ovary in adult female albino rats? (Histological and immunohistochemical study). Stem Cell Res. Ther. 8, 442. https://doi.org/10.4172/2157-7633.1000442.
Gallagher, M., Rebecca, B., Margaret, B., 2015. Severity of Spatial Learning Impairment in Aging: Development of a Learning Index for Performance in the Morris Water Maze, p. 540.
Gitler, A.D., Dhillon, P., Shorter, J., 2017. Neurodegenerative disease: models, mechanisms, and a new hope. Dis. Model. Mech. 10, 499–502 [CrossRef] [PubMed].
Go, J., Kim, J.E., Kwak, M.H., Koh, E.K., Song, S.H., Sung, J.E., Kim, D.S., Hong, J.T., Hwang, D.Y., 2016. Neuroprotective effects of fermented soybean products (Cheonggukjang) manufactured by mixed culture of Bacillus subtilis MC31 and Lactobacillus sakei 383 on trimethyltin-induced cognitive defects mice. Nutr. Neurosci. 19 (Jul (6)), 247–259.
Gorgun, C., Reverberi, D., Rotta, G., Villa, F., Quarto, R., Tasso, R., 2019. Isolation and flow cytometry characterization of extracellular-vesicle subpopulations derived from human mesenchymal stromal cells. Curr. Protoc. Stem Cell Biol. 48, e76. https://doi.org/10.1002/cpsc.76.
Hämäläinen, A., Grau-Olivares, M., Tervo, S., Niskanen, E., Pennanen, C., Huuskonen, J., Kivipelto, M., Hänninen, T., Tapiola, M., Vanhanen, M., Hallikainen, M., 2008. Apolipoprotein E ε4 allele is associated with increased atrophy in progressive mild cognitive impairment: a voxel-based morphometric study. Neurodegener. Dis. 5(3–4), 186–189.
Harris, V.K., Stark, J., Vyshkina, T., Blackshear, L., Joo, G., Stefanova, V., Sara, G., Sadiq, S.A., 2018. Phase I trial of intrathecal mesenchymal stem cell-derived neural progenitors in progressive multiple sclerosis. EBioMedicine 29, 23–30. https://doi.org/10.1016/j.ebiom.2018.02.002, 2018.
Hatters, D.M., 2008. Protein misfolding inside cells: the case of huntingtin and Huntington's disease. IUBMB Life 60, 724–728. https://doi.org/10.1002/iub.111.
Hervas, R., Oroz, J., Galera-Prat, A., Goni, O., Valbuena, A., Vera, A.M., Gomez-Sicilia, A., 2012. Common features at the start of the neurodegeneration cascade. PLoS Boil. 10, e1001335 [CrossRef] [PubMed].
Hussain, R., Zubair, H., Pursell, S., Shahab, M., 2018. Neurodegenerative diseases: regenerative mechanisms and novel therapeutic approaches. Brain Sci. 8 (9), 177.
Jackson, P., Blythe, D., 2013. Immunohistochemical techniques [Chapter 18]. In: Suvarna, S.K., Layton, C., Bancroft, J.D. (Eds.), Theory and Practice of Histological Techniques, 7th ed. Churchill Livingstone of Elsevier, Philadelphia, pp. 381–426.
Kumar, G., Kiernan, J.A., 2010. Education Guide, Special Stains and H&E, 2nd ed., p. 67 Chapter 8. North America, Carpinteria, California: staining sections of the central nervous system.
Lepeta, K., Lourenco, M.V., Schweitzer, B.C., Martino Adami, P.V., Banerjee, P., Catuara-Solarz, S., de La Fuente Revenga, M., Guillem, A.M., Haidar, M., Ijomone, O.M., 2016a. Synaptopathies: synaptic dysfunction in neurological disorders—A review from students to students. J. Neurochem. 138, 785–805.
Lepeta, K., Lourenco, M.V., Schweitzer, B.C., Martino Adami, P.V., Banerjee, P., Catuara-Solarz, S., de La Fuente Revenga, M., Guillem, A.M., Haidar, M., Ijomone, O.M., 2016b. Synaptopathies: synaptic dysfunction in neurological disorders—A review from students to students. J. Neurochem. 138, 785–805. https://doi.org/10.1111/jnc.13713.
Minett, T., Classey, J., Matthews, F.E., Fahrenhold, M., Taga, M., Brayne, C., Ince, P.G., Nicoll, J.A., Boche, D., CFAS, M., 2016. Microglial immunophenotype in dementia with Alzheimer's pathology. J. Neuroinflammation 13 (Dec (1)), 135, 2016.
Montero-Odasso, M., Pieruccini-Faria, F., Bartha, R., Black, S.E., Finger, E., Freedman, M., Greenberg, B., Grimes, D.A., Hegele, R.A., Hudson, C., 2017. Motor phenotype in neurodegenerative disorders: gait and balance platform study design protocol for the Ontario neurodegenerative research initiative (ONDRI). J. Alzheimer's Dis. 59, 707–721 [CrossRef] [PubMed].
Nakano, M., Nagaishi, K., Konari, N., Saito, Y., Chikenji, T., Mizue, Y., Fujimiya, M., 2016. Bone marrow-derived mesenchymal stem cells improve diabetes-induced cognitive impairment by exosome transfer into damaged neurons and astrocytes. Sci. Rep. 6, 24805 (2016) [PMC free article] [PubMed].
Nassar, W., El-Ansary, M., Sabry, D., et al., 2016. Umbilical cord mesenchymal stem cells derived extracellular vesicles can safely ameliorate the progression of chronic kidney diseases. Biomater. Res. 20 (21) https://doi.org/10.1186/s40824-016-0068-0 (PMCID: PMC4974791).
Phinney, D.G., Pittenger, M.F., 2017. Concise review: MSC-derived exosomes for cell-free therapy. Stem Cells 35, 851–858 (2017) [PubMed] [Google Scholar.
Qu, J., Zhang, H., 2017. Roles of mesenchymal stem cells in spinal cord injury. Stem Cells Int., 5251313 https://doi.org/10.1155/2017/5251313.
Reza-Zaldivar, E.E., Hernández-Sapiéns, M.A., Gutiérrez-Mercado, Y.K., Sandoval-Ávila, S., Gomez-Pinedo, U., Marquez-Aguirre, A.L., Vázquez-Méndez, E., Padilla-Camberos, E., Canales-Aguirre, A.A., 2019. Mesenchymal stem cell-derived exosomes promote neurogenesis and cognitive function recovery in a mouse model of Alzheimer's disease. Neural Regen. Res. 14 (Sep (9)), 1626–1634. https://doi.org/10.4103/1673-5374.255978.
Rong, W., Ding, K., Guo, S., Xie, F., Li, Q., Bi, K., 2019. Metabolomics analysis of Xanthoceras sorbifolia husks protection of rats against Alzheimer disease using liquid chromatography mass spectrometry. J. Chromatogr. B Analyt. Technol. Biomed. Life Sci. (Sep), 1126–1127. https://doi.org/10.1016/j.jchromb.2019.121739, 121739.
Sawyer, R.P., Rodriguez-Porcel, F., Hagen, M., et al., 2017. Diagnosing the frontal variant of Alzheimer's disease: a clinician's yellow brick road. J. Clin. Mov. Disord. 4, 2. https://doi.org/10.1186/s40734-017-0052-4.
Scuteri, A., Donzelli, E., Foudah, D., Caldara, C., Redondo, J., D'Amico, G., Tredici, G., Miloso, M., 2014. Mesengenic differentiation: comparison of human and rat bone marrow mesenchymal stem cells. Int. J. Stem Cells 7, 127–134. https://doi.org/10.15283/ijsc.2014.7.2.127.
Shahror, R.A., Ali, A.A., Wu, C., Chiang, Y.H., Chen, K.Y., 2019. Enhanced homing of mesenchymal stem cells overexpressing fibroblast growth factor 21 to injury site in a mouse model of traumatic brain injury. Int. J. Mol. Sci. 20 (11), 2624. https://doi.org/10.3390/ijms20112624.
Shwe, T., Pratchayasakul, W., Chattipakorn, N., Chattipakorn, S.C., 2018. Role of D-galactose- induced brain aging, and its potential used for therapeutic interventions. Exp. Gerontol. 101 (Jan), 13–36. https://doi.org/10.1016/j.exger.2017.10.029.
Teixeira, C.P., Florencio-Silva, R., Sasso, G.R.S., Carbonel, A.A.F., Simões, R.S., Simões, M.J., 2019. Soy isoflavones protect against oxidative stress and diminish apoptosis in ovary of middle-aged female rats (2019). Gynecol. Endocrinol. 35 (Jul (7)), 586–590. https://doi.org/10.1080/09513590.2018.1559287.
Théry, C., Amigorena, S., Raposo, G., Clayton, A., 2006. Isolation and characterization of exosomes from cell culture supernatants and biological fluids. Curr. Protoc. Cell Biol. 30 (Mar (1)), 3–22.
United Nations DoEaSA, 2017. Population Division. World Population Ageing 2017 — Highlights (ST/ESA/SER.A/397).
Vadakkan, Kunjumon I., 2016. Neurodegenerative disorders share common features of "loss of function" states of a proposed mechanism of nervous system functions. Biomed. Pharmacother. Biomed. Pharmacother. 83, 412–430 [CrossRef] [PubMed].
Waller, R., Baxter, L., Fillingham, D.J., Coelho, S., Pozo, J.M., Mozumder, M., Frangi, A. F., Ince, P.G., Simpson, J.E., Highley, J.R., 2019. Iba-1-/CD68+ microglia are a

prominent feature of age-associated deep subcortical white matter lesions. PLoS One 14 (1).
Woolley, J.D., Khan, B.K., Murthy, N.K., Miller, B.L., Rankin, K.P., 2011. The diagnostic challenge of psychiatric symptoms in neurodegenerative disease: rates of and risk factors for prior psychiatric diagnosis in patients with early neurodegenerative disease. J. Clin. Psychiatry 72, 126–133 [CrossRef] [PubMed].
Xi, Y.D., Li, X.Y., Ding, J., Yu, H.L., Ma, W.W., Yuan, L.H., Wu, J., Xiao, R., 2013. Soy isoflavone alleviates Aβ1induced impairment of learning and memory ability through the regulation of RAGE/LRP-1 in neuronal and vascular tissue. Curr. Neurovasc. Res. 10 (May (2)), 144–156. https://doi.org/10.2174/1567202611310020007.
Xi, Y.D., Li, X.Y., Yu, H.L., Jing, H., Ma, W.W., Yuan, L.H., Zhang, D.D., Wu, J., et al., 2014. Soy isoflavone antagonizes the oxidative cerebrovascular injury induced by β-amyloid peptides 1–42 in rats. Neurochem. Res. 39 (7), 1374–1381. https://doi.org/10.1007/s11064-014-1319-x. Neurochem Res. 2014 Jul; 39 (7): 1374-1381.
Xu, C., Shu, W.Q., Qiu, Z.Q., Chen, J.A., Zhao, Q., Cao, J., 2007. Protective effects of green tea polyphenols against subacute hepatotoxicity induced by microcystin-LR in mice. Environ. Toxicol. Pharmacol. 24, 140–148. https://doi.org/10.1016/j.etap.2007.04.004.
Yang, J., Zhang, X., Chen, X., Wang, L., Yang, G., 2017a. Exosome mediated delivery of miR-124 promotes neurogenesis after ischemia. Mol. Ther. Nucleic Acids 7, 278–287 (2017) [PMC free article] [PubMed] [Google Scholar].
Yang, Y., Ye, Y., Su, X., He, J., Bai, W., He, X., 2017b. MSCs-derived exosomes and neuroinflammation, neurogenesis and therapy of traumatic brain injury. Front. Cell. Neurosci. 11, 55 (2017) [PMC free article][PubMed] [Google Scholar].
Yentrapalli, R., Merl-Pham, J., Azimzadeh, O., Mutschelknaus, L., Peters, C., Hauck, S.M., Atkinson, M.J., Tapio, S., Moertl, S., 2017. Quantitative changes in the protein and miRNA cargo of plasma exosome-like vesicles after exposure to ionizing radiation. Int. J. Radiat. Biol. 93 (Jun (6)), 569–580.
Zhang, X., Zhang, H., Xia, X., Pu, N., ZhupingYu, Z., Nabih, M., Zhu, Y., Zhang, S., Jiang, L., 2019. Preparation and physicochemical characterization of soy isoflavone (SIF) nanoparticles by a liquid antisolvent precipitation method. Adv. Powder Technol. 30, 1522–1530. https://doi.org/10.1016/j.apt.2019.04.030.